

Molecular Insight into the Effect of a Single-Nucleotide Polymorphic Variation on the Structure and Dynamics of Methionine Synthase Reductase and Its Association with Neural Tube Defects

Susanta Sadhukhan, Subhajit Maity, Sandipan Chakraborty, Silpita Paul, Dinesh Munian, Arup Kumar Pattanayak, Biman Jana,* and Madhusudan Das*



Cite This: *ACS Omega* 2021, 6, 26372–26380



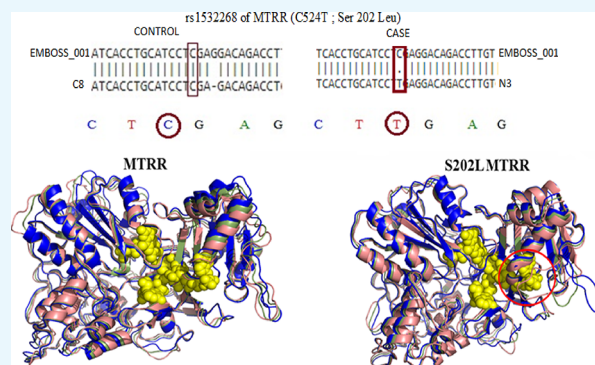
Read Online

ACCESS |

Metrics & More

Article Recommendations

ABSTRACT: Neural tube defects (NTDs) are among the common and severe congenital malformations in neonates. According to a WHO report, nearly three lakh babies are affected per year worldwide by NTDs. Most studies revealed that folate deficiency is the key element to promote NTD with other oligogenic and multifactorial elements. This folate is metabolized by the FOCM (folate one-carbon metabolism) pathway. The most important step in the FOCM pathway is the conversion of methionine to homocysteine, which is guided by the enzyme MTRR. Several single-nucleotide polymorphisms (SNPs) in the *MTRR* gene are strongly associated with the progression of NTD. A nonsynonymous allelic variant (rs1532268) of the protein leads to a missense mutation at the 202nd position from serine to leucine (S202L) and is associated with a higher disease prevalence in different populations. In our study, this SNP indicates a 2-fold increase in the risk of disease progression (p -value of 0.03; OR 2.76; 95% CI 1.08–7.11). Here, extensive molecular dynamics simulations and interaction network analysis reveal that the change of 202nd serine to leucine alters the structures of the FAD and NAD binding domains, which restricts the ligand binding. The S202L variation alters the functional dynamics that might impede the electron transport chain along the NADP(H) FAD FMN pathway and hamper phosphorylation by kinases like GSK-3 and CaM-II during the posttranscriptional modification of the protein. The present study provides functional insights into the effect of the genetic variations of the *MTRR* gene on the NTD disease pathogenesis.



1. INTRODUCTION

Neural tube defects (NTDs) are among the deadliest congenital and inborn malfunctions affecting our central nervous system (i.e., brain and spinal cord).¹ The occurrence and prevalence of NTDs range from 0.5 to 11 per 1000 births in various regions of the Indian subcontinent.² A neural tube or neurulation formation is a complicated developmental process governed by many genes, receptors, and specific growth factors.^{3,4} NTD can be categorized into spina bifida and anencephaly, based on the positional deformities within the central nervous system. The affected children either have paralysis or immobile life with urinogenital and cardiological problems.^{5,6} There are no treatments available for infants with extreme anencephalic conditions. Research indicates that both the genetic and environmental factors are responsible for the observed disease etiology.^{7–9} The fatal disease is influenced by age, ethnicity, race, location, socio-economic status, and nutritional status.^{10,11} Among them, the nutrient status during pregnancy in mothers is a critical determinant related to disease pathogenesis. There is a strong association between

folate acid metabolism and neural tube defects.^{12–14} Folate is required for the synthesis of new cells and also for the running of the central dogma. It is also needed to carry out one-carbon group addition for methylation and biosynthesis of nucleic acids.¹⁵ Therefore, exogenous folate is essential for the housekeeping maintenance of the cell. It was observed that folic acid supplementation during pregnancy reduces the prevalence of NTDs in newborns.¹⁶ However, the mechanism is yet to be understood. There is a strong genetic rationale behind the NTD disease prevalence within a population⁴ as certain individuals are at greater risk. Several genetic studies demonstrated that family history and ethnicity significantly

Received: July 6, 2021

Accepted: September 17, 2021

Published: September 30, 2021



impact the disease prevalence. Due to strong associations between folate status and NTD risk, identifying the genetic risk factors involved in the transport, process, and metabolism of folic acid is a topic of intense research interest.

The *MTRR* gene encodes the methionine synthase reductase. The methionine synthase enzyme catalyzes methionine synthesis.¹⁷ However, the enzyme becomes inactive during the process due to the oxidation of its cobalamin cofactor. Methionine synthase reductase regenerates functional methionine synthase via the process of reductive methylation.¹⁸ The enzyme causes reductive methylation of homocysteine to methionine, utilizing the methyl-cob(I)-alamin as a paratenic methyl carrier. An electron transport chain mediates the reduction derived from NADPH oxidation and proceeds via the FAD (flavin adenine dinucleotide) to FMN (flavin mononucleotide), the redox center of *MTRR*.¹⁸ The *MTRR* gene polymorphism leads to interindividual genetic differences that can be translated and correlated into abnormal folate metabolism.¹⁹ This error in metabolism can be considered a crucial cause for the development of NTDs. Polymorphisms in the *MTRR* gene are strongly influenced by the ethnic and geographic origins of the population. Therefore, genetic risk factor associations between the *MTRR* gene and NTDs may vary among populations. However, only a few studies were previously carried out to correlate *MTRR* genetic variations with the prevalence of NTDs in the Indian population, particularly in the Eastern region of the country. We performed a genetic association study of neural tube defects with the spectrum and frequencies of *MTRR* gene variation based on the population of Eastern India. We showcased the association of rs1801394 (I49M) in the *MTRR* gene with the complications of NTDs.²⁰ An allelic variant of this protein leads to a missense mutation at the 49th position from isoleucine to methionine, which is associated with a higher disease prevalence in different populations. Extensive molecular dynamics simulations and interaction network analysis revealed that the 49th isoleucine is a crucial residue that allosterically regulates the dynamics between the flavin mononucleotide (FMN) and NADP(H) binding domains. The I49M variation altered that functional dynamics as evident from the structural insights of the protein.²⁰

In the present study, we have mainly focused on screening the single-nucleotide polymorphic structural variation of methionine synthase reductase (*MTRR*) and its association with neural tube defects by exploiting a combination of genetic screening and various computational approaches.

2. RESULTS AND DISCUSSION

2.1. Characteristics of the Study Cohorts. Our previous study separately tabulated all the detailed screening parameters and striking characteristics of our study cohorts (both case and control mothers).²¹ The folic acid level in the blood was significantly different between control (12.81 ± 4.47 ng/mL) and case mothers (8.98 ± 1.63 ng/mL; control vs case, *p*-value of <0.0001), but the serum Hcy concentration did not exhibit any significant change between case or control groups (*p*-value: 0.338).

2.2. Genotyping Study in Case and Control Cohorts. Allele frequencies of rs1532268 of the *MTRR* gene (C524T; S202L) have been decoded and delineated in Table 1 and Figure 1. The minor allele T frequencies for both case and control are 59 and 58%, respectively. For the same rs1532268, the C allele frequencies of both the case and control are 41 and

Table 1. Allele and Genotype Frequencies of the *MTRR* rs1532268 Association with the NTD Risk

SNPs	allele	allele frequency	odds ratio (95% CI) ^a	<i>p</i> -value ^b	<i>p</i> -value (H–W equilibrium)	genotype	case (n = 62)	control (n = 73)	odds ratio (95% CI) ^c	<i>p</i> -value
MTRR C524T;rs1532268Ser 202 Leu	C	case (%) 41	1.04 (0.59–1.83)	0.886	case 0.067	CC	7 (11.3%)	19 (26%)	reference	0.03
	T	59				CT	37 (59.7%)	24 (32.9%)	AA vs AG + GG dominant	
				TT	18 (29%)	30 (41.0%)	AA + AG vs GG recessive	0.145		

^aOdds ratio adjusted by age. ^b*p*-value adjusted by age and *p*-value less than 0.05 denoted in italics along with the “*p*” of *p* value (according to convention). ^cConfidence interval.

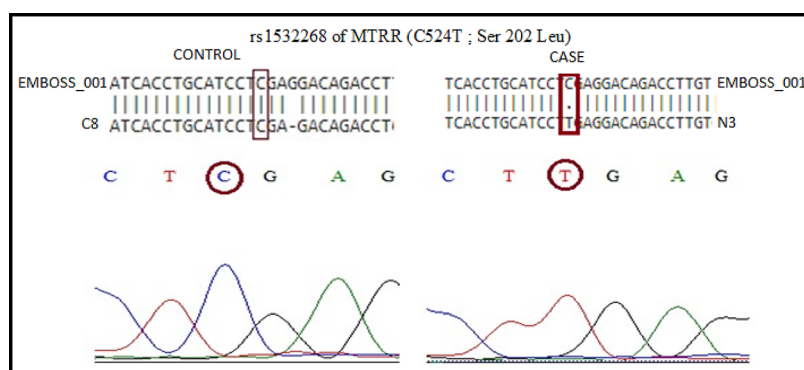


Figure 1. Comparative MTRR sequencogram in control and case populations.

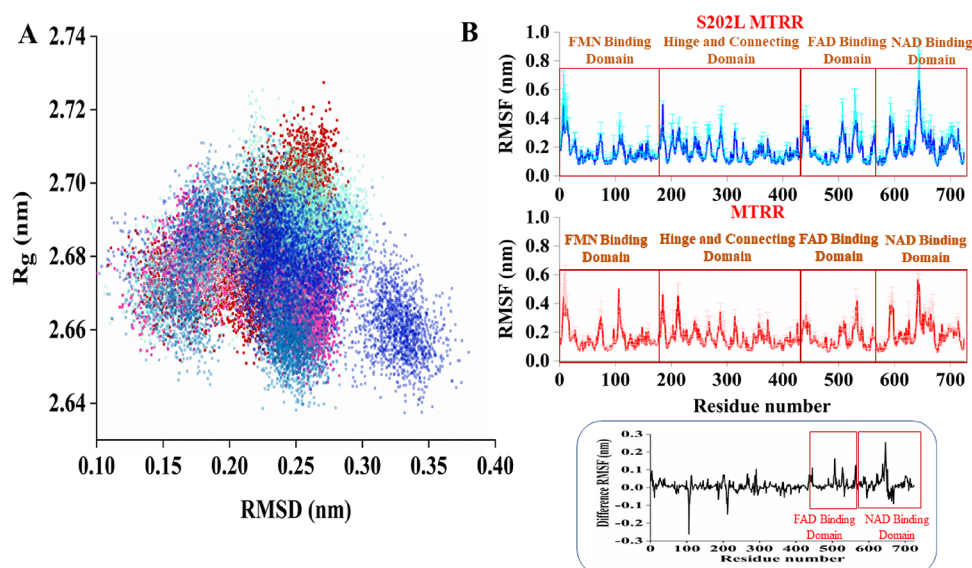


Figure 2. (A) 2D scatter plot of RMSD and R_g of the MTRR (red) and its S202L variant (blue) from three independent 500 ns simulations. (B) Root mean square fluctuations of the wild-type (lower panel) and S202L MTRR variants, observed from equilibrium simulations. Results are presented in terms of mean \pm SD obtained from three independent simulations. The difference RMSF plot (S202L MTRR–wild type MTRR) is shown below within the inset where the FAD and NAD binding regions are highlighted.

42%, respectively. The allelic model fails to show any statistical significance (OR of 1.04; 95% CI 0.59–1.83; p -value of 0.886). On the other hand, the genotype frequencies for case and control are CC = 11.3%; 26%, CT = 59.7%; 32.9% and TT 29%; 41%, respectively. The genotypic dominant statistical model shows a 2-fold increased risk for NTD (p -value of 0.03; OR 2.76; 95% CI 1.08–7.11). In conclusion, our study indicates that the TT genotype for rs1532268 of MTRR seems to be a useful marker for susceptibility of NTDs in the Indian population.

2.3. S202L Variation Alters the Structure and Dynamics of the MTRR. We have used extensive molecular dynamics simulations to understand the effect of Ser202Leu (S202L) variation on the structure and dynamics of the protein. We have considered two global structural parameters, root mean square deviations (RMSD) and radius of gyration (R_g), to probe the conformational landscape of the wild-type and S202L MTRR variants from three independent 500 ns simulations for each system, and the results are shown in Figure 2A.

Evident from the figure, the wild-type protein is more stable and confined within a narrower region of the 2D conformational landscape defined by the RMSD and R_g . The maximum

observed RMSD is ~ 2.5 Å with respect to the initial conformation of the protein. On the other hand, R_g spans over 2.66–2.72 nm. The results signify high stabilization of the wild-type MTRR structures during the simulation timescale for all the replicas. However, the S202L variant displays increased fluctuations during the simulation. The RMSD for the variant reaches up to ~ 3.5 Å with respect to the initial conformation during the simulation timescale. However, the R_g remains comparable to the wild-type MTRR throughout the simulation timescale. Thus, S202L alteration changes the conformational dynamics of the protein. We then investigated the role of S202L substitution in the residue fluctuations (Figure 2B). The residue 202 locates at the hinge region that connects the FMN domain to the connecting domain. However, the root mean square fluctuation (RMSF) calculation based on all the simulation trajectories reveals that high fluctuations are observed in other regions, particularly the long distant FAD and NAD binding domains (Figure 2B, inset). This observation indicates that the residue is possibly a part of the allosteric network that allows communication between several distant domains through an interaction network. Alteration of the residue leads to an altered interaction

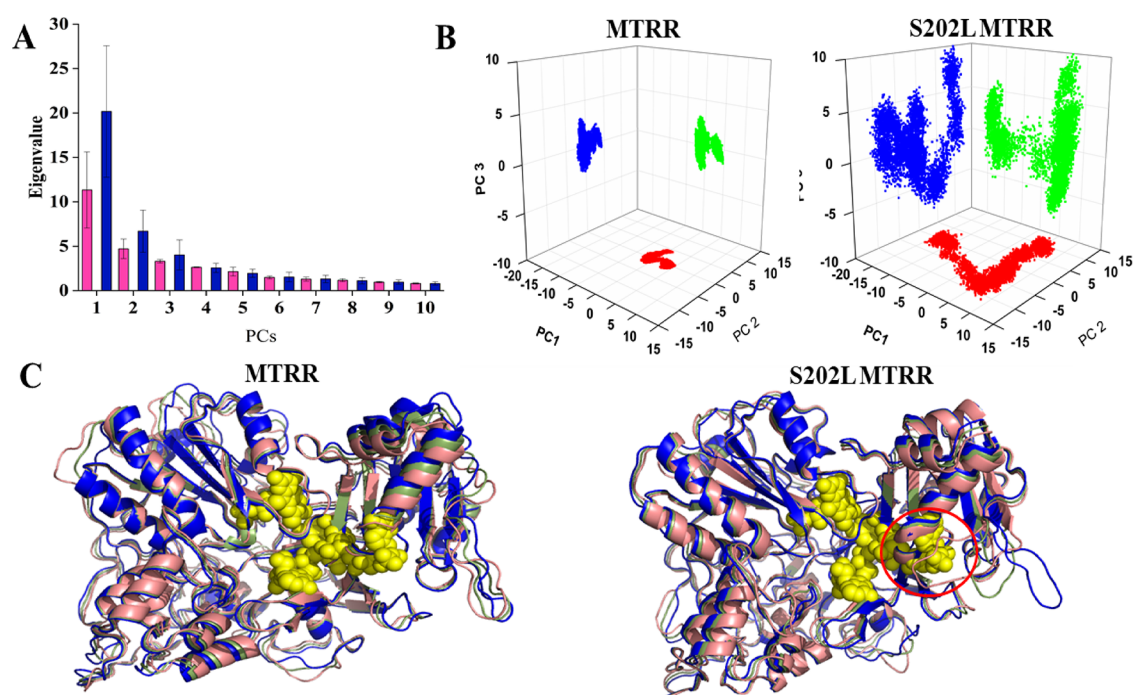


Figure 3. (A) Distribution of eigenvalues of the first 10 principal components obtained from the PCA analysis of all the simulation trajectories of MTRR (pink) and S202L variant (blue). (B) 2D projections of the first three principal components of MTRR (left side) and S202L MTRR (right side), obtained from the molecular dynamics simulation. (C) Essential dynamics of the wild-type MTRR and its S202L variant obtained by simulating the protein along the first principal component (PC1) derived from the covariance analysis of the simulation trajectories are shown. Proteins are rendered in cartoon mode. Three conformations of the protein have been generated by simulating both the proteins along PC1 and colored consecutively as salmon, tan, and blue cartoons. NADP(H), FAD, and FMN are colored in yellow vdW representation. The sterically clashed region is shown in the red circle.

network that hinders the allosteric communication, which resulted in altered dynamics of the different domains.

Motions observed in the molecular dynamics simulation are very complex to decode, as small-scale motions are clubbed with large-scale domain movements. Thus, it is imperative to identify large-scale motions from the simulation trajectories, as the large-scale collective dynamics generally provide crucial information on the functional motions of the protein. Principal component analysis (PCA) is an effective way to decode the functional motions of the protein from the simulation trajectory,^{22–24} and the first few principal components generally dictate the high amplitude collective motions of the protein.

The distribution of eigenvalues of the principal components (PCs) obtained from the PCA analysis of MTRR and S202L MTRR simulation trajectories reveals that the first three components are associated with high eigenvalues. Therefore, the first few PCs account for most of the dynamics observed from the molecular dynamics simulation. The 2D projections of both MTRR and S202L MTRR conformations along the first three PCs are shown in Figure 3B. Evident from the figure, the protein dynamics are confined in the essential subspace for MTRR. The projection of the S202L variant is widely distributed. The PC1 explains most of the variance of the covariance matrix for both MTRR and S202L MTRR. Thus, we have studied the essential dynamics of both the wild-type and variant MTRR by simulating the protein along with the first principal component, and the results are shown in Figure 3C. The observed motions of the wild-type MTRR along the PC1 are highly cooperative. Several domains move together to produce the functional transitions. The FAD binding domain

and connecting domain remain less flexible. However, several loopy regions show considerable flexibility. Remarkably, a cooperative movement between the FMN and NADP(H) binding domains is observed where both the domains move close to each other. Binding site volume calculation using the PockDrug²⁵ web server showed that the simulation of the wild-type MTRR along the PC1 leads to cavity closure where the cavity volume reduced from 31,422 to 22,514 Å³. Since the ligand-bound full-length structure of the MTRR is yet to be resolved, we have aligned the ligand-bound structure of NADPH–cytochrome P450 oxidoreductase (PDB ID: 1JA0),²⁶ a close homolog of MTRR. The coordinates of all the three bound ligands (NADP(H), FAD, and FMN) were obtained and placed within the binding sites of MTRR and its S202L variant to understand the functional significance of the motion. Evident from the figure (Figure 3C, left panel), in the case of the wild-type MTRR, the domain movement leads to a close association between the NADP(H), FAD, and FMN, which facilitates the electron transport chain along the NADP(H) FAD FMN pathway.

The functional dynamics of the S202L variant along the PC1 are drastically different from those of the wild-type MTRR. Evident from Figure 3C (right panel), the FMN and NADP(H) binding domains are highly dynamic, which is in substantial agreement with the RMSF plot (Figure 2B). The loop regions of the FAD and NADP(H) region that frame the cofactor binding cavity are highly flexible. The movement of the loops sterically restricts the ligand binding (Figure 3C, right panel, within the circle).

We then performed cluster analysis to identify the most probable solution structures of MTRR and its S202L variant.

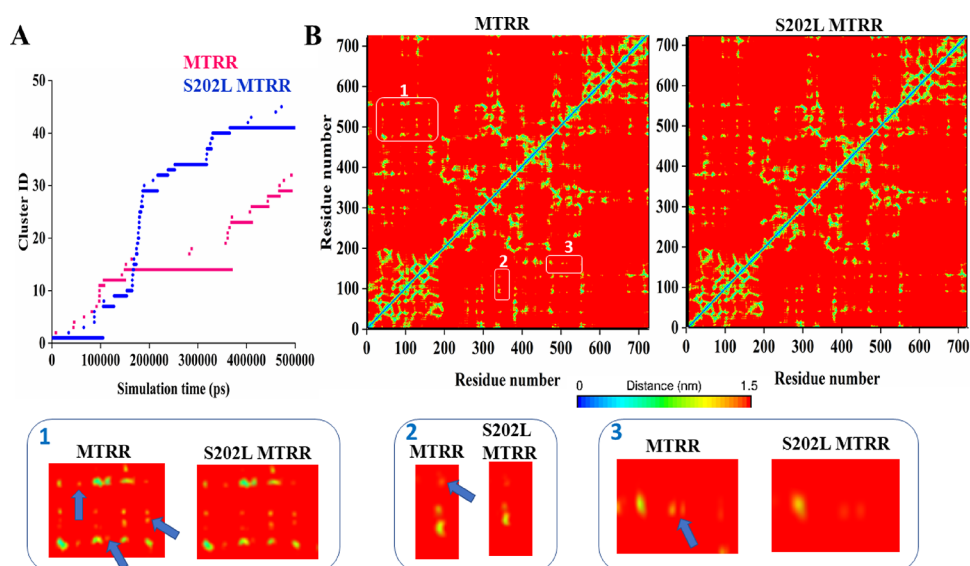


Figure 4. (A) Distribution of clusters over the entire trajectory for MTRR (red) and S202L MTRR variant (blue). (B) Mean 2D contact map of all protein atoms for MTRR and its S202L variant obtained from a 500 ns simulation trajectory. Each of the three highlighted regions for MTRR and S202L MTRR is zoomed and shown below within the inset. Changes are indicated with the arrow.

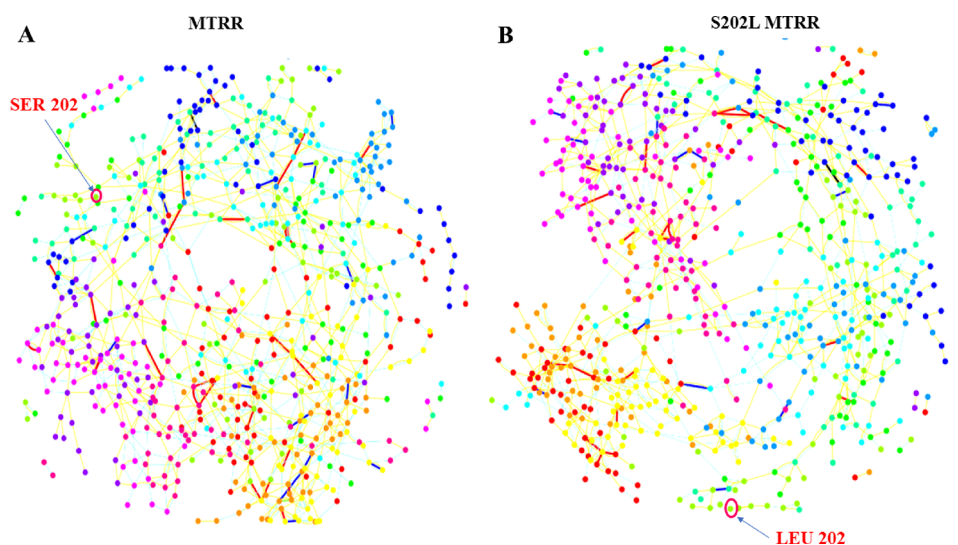


Figure 5. Residue–residue connectivity map of the average structure obtained from the most populated conformational cluster of wild-type (A) and S202L MTRR (B).

We have used a 1.1 Å $C\alpha$ RMSD cutoff for clustering. Evident from the cluster distribution (Figure 4A), the number of different conformational clusters for MTRR visited during the simulation is significantly lower than that during the S202L MTRR simulations. The conformations obtained from the entire 500 ns simulation trajectory of the wild-type MTRR are grouped into 32 clusters, and cluster 14 is the most populated one. Meanwhile, for S202L MTRR, all the conformations observed from the simulation are grouped into 45 clusters. Among them, the 41st cluster is the most populated one.

The mean 2D contact map of all protein atoms for MTRR and its S202L variant obtained from a 500 ns simulation trajectory is shown in Figure 4B. The critical difference between the two contact maps is highlighted within a square. Long-distance contacts between the FMN and FAD binding domains and the FMN and hinge regions are more evident from the wild-type MTRR simulation than the S202L variant (Figure 4B, lower inset). Thus, the alteration at the 202nd

position causing changes in some long-distance interdomain communication might hamper the functional dynamics of the protein.

To probe the effect of the serine to leucine variation on the intraprotein interaction network, we have further characterized the residue–residue connectivity map of the structure obtained from the most populated conformational cluster of wild-type and S202L MTRR using the RING web server.²⁷ Evident from Figure 5, Serine202 belongs to a network pathway that allosterically controls interdomain communications, which is essential to regulate the functional motion of the protein. The serine to leucine variation at the 202nd position allows the formation of a local hydrophobic cluster with Leu211, Leu212, and Ile214 that remodel the allosteric network. Leu202 is no more part of the intraprotein interaction network. Instead, it exists as a segregated node. Thus, alteration of the intraprotein network can significantly affect the allosteric communications

between different domains during the functional dynamics of the protein.

2.4. S202L Alteration Can Affect Posttranslational Modification. The SNP variation leads to a change of the serine residue of the MTRR. Serine is a crucial residue for posttranslational modification sites. Therefore, we have critically analyzed the possible posttranslational modification sites of the wild-type MTRR protein. Results are summarized in Table 2. Serine202 is a crucial residue for phosphorylation

Table 2. List of Possible Predicted Phosphorylation and Sumoylation Sites of MTRR

probable phosphorylation site (score)	specific kinases	sumoylation site (<i>p</i> -value)
SER 202 (0.996)	GSK-3, CAM-II	LYS 74 (0.003)
SER 184 (0.995)	PKA, PKC	LYS 208 (0.005)
SER 535 (0.995)	GSK-3, CAM-II	LYS 714 (0.003)
SER 183 (0.991)	GSK-3, CAM-II	
SER 293 (0.985)	CAM-II	
SER 539 (0.985)	GSK-3	
SER 422 (0.983)	GSK-3	
SER 635 (0.962)	Cdc2, PKC	
SER 550 (0.948)	p38MAPK	
SER 333 (0.931)	cdc2	
SER 66 (0.902)	CKII	

by kinases like GSK-3 and CaM-II, as predicted by NetPhosK 1.0²⁸ and NetPhos 2.0.²⁹ Other relevant phosphorylation sites and possible kinases are listed in the table.

Prediction of other possible posttranslational modification sites also reveals that a nearby lysine residue, Lys208, is a highly probable sumoylation site. If alteration of serine to leucine at the 202nd position alters the local structure, it can also impact the sumoylation of the nearby Lys208 residue.

3. CONCLUSIONS

The congenital neural tube defect (NTD) occurs at a high prevalence in India and the world (0.5–11 per 1000 births). Several genes, specific growth factors, age, ethnicity, race, location, socio-economic condition, and nutritional status contribute significantly to the disease prevalence. Treatments of NTD depend on the severity of the diseased infants. In the case of an extreme anencephalic condition, the treatment is entirely lacking. Therefore, identifying genetic markers and genetic counseling help early detection, percussion, and proper monitoring of the fetus.

The polymorphisms of folate metabolism pathway genes can evoke several human congenital disabilities. We, herein, carried out a screening program in the population of West Bengal, India, to find out the distribution of some specific SNPs that were reported earlier as a probable cause of NTDs. Pishva *et al.*³⁰ (from the Pediatric Infectious Research Center, PIRC) reported that Tehran–Iranian shows a modest association of rs1532268 with patients with congenital heart disease (CHD). In contrast, the association of this rs1532268 with several other diseases is still ambiguous. The present study is the first report from Eastern India to depict the association between the rs1532268 and NTDs. Notably, significant variations are observed at the genotypic level. The CT genotype frequency for the case is higher than the control, whereas the TT

genotype is lower in the case studies (CT = 59.7%/32.9% and TT = 29%/41% for case and control, respectively). Therefore, the genotypic dominant statistical model shows a 2-fold increase in the risk of NTD progression (*p*-value of 0.03; OR 2.76; 95% CI 1.08–7.11). Our study indicates that the CT genotype for rs1532268 of MTRR seems to be a helpful marker for susceptibility to NTD. To the best of our knowledge, this is the first study reported from the Eastern part of India that mapped the allele and genotype frequency distribution and rs1532268. Hence, our study can function as a platform for future studies to evaluate the association of NTD with the variant in MTRR genes in an ethnically distinct population.

The nonsynonymous allelic variation (rs1532268) of the protein leads to a missense mutation at the 202nd position from serine to leucine (S202L). We have used extensive molecular dynamics simulation to characterize the functional effect of S202L variation on the structure and dynamics of the MTRR protein. This change alters the long-distance interdomain contacts by modulating the allosteric movement among the FMN, FAD, and NADP(H) binding domains. Essential dynamics reveal that S202L alteration induces high fluctuations in several loop regions that mainly frame the NADP(H) binding site. The movement of the loops sterically restricts the ligand binding, thereby perturbing the electron transport chain along the NADP(H) FAD⁺ FMN pathway. Also, we predict that the 202nd serine is a critical residue for phosphorylation by kinases like GSK-3 and CaM-II. Changes of the residue to leucine alter the posttranslational modification of the protein. Posttranslational modification is essential for the proper function and localization of the protein. Our study reveals that the S202L variation impedes both the posttranslational maturation and functional dynamics of the protein, MTRR, which catalyzes methionine biosynthesis.

Here, we also present a multidisciplinary approach to explore the functional effect of a nonsynonymous allelic variant. The application of extensive molecular dynamics simulation and essential dynamics allow us to reveal the mechanism of the functional aberration of the protein due to an allelic variation at an atomic resolution, which is very challenging to probe experimentally. Therefore, the present study also highlights the applicability of molecular dynamics simulation and bioinformatics to screen out highly significant genetic markers for better disease prognosis.

4. EXPERIMENTAL SECTION

4.1. Study Sample. All the samples (case, *n* = 62; control, *n* = 73) were collected from the Department of Neonatology of Seth Sukhlal Karnani Memorial Hospital (SSKM) and the Institute of Post-Graduate Medical Education and Research (IPGMER), Kolkata, India, during the period of January 2014–August 2017 with prior ethical approval (memo no. Inst/IEC/2015/43). Case mothers in the present study gave birth to babies with spina bifida, anencephaly, or hydranencephaly. Control mothers were undoubtedly considered as normal as they gave birth to healthy ones. Diabetic mothers were not considered in both the study cohorts (i.e., case and control), as some research reports showed minor associations between NTDs and diabetes. Some other inclusion criteria for the case and exclusion for control were followed according to Paul *et al.*²¹ Socio-economic condition, occupation of parents, smoking and drinking habits, regular food habit, folate intake during pregnancy, pregnancy term, diabetes, and previous

family history with NTDs or any other congenital disabilities were also scrutinized.

4.2. Biochemical Study. The chemiluminescent micro-particle immunoassay (CMIA) of the Architect Plus system (Abbott, Germany) was used to measure serum folic acid (reference range 4–20 ng/mL; University of California, San Francisco; 2018). An enzymatic assay technique was used to measure homocysteine (Diazyme, USA) (reference concentration, i.e., <15 $\mu\text{mol/L}$; University of California, San Francisco; 2018).

4.3. Genotyping. DNA was isolated from all the case and control samples using the QIAamp Blood Kit (QIAGEN, Hilden, Germany). The concentrations and purity of DNA were measured in each sample using a nanophotometer (absorbance at 260 and 280 nm, respectively). Polymerase chain reactions (PCR) were done using the PCR mixture and cycling program in a thermocycler for standardizing specific exon-containing mentioned SNPs. The reaction mixture was prepared in a 25 μL volume. The mixture composition was 40–100 ng of genomic DNA, 1.5 mM MgCl_2 , 100 μM of each dNTPs, 0.4 μM of each primer, and 0.5 unit of Taq DNA polymerase (Applied Biosystems). For amplification of the particular SNP within the thermocycler, it followed the denaturation at 95 $^\circ\text{C}$ for 30 s, annealing at 58 $^\circ\text{C}$ for 30 s, and extension at 72 $^\circ\text{C}$ for 30 s (for consecutive 42 cycles). A 1.5% agarose gel electrophoresis technique was used to identify the PCR product size. The PCR product of the particular SNP was sequenced using a Taq Dye Deoxy Terminator sequencing kit (Applied Biosystems, USA, with an ABI Prism 377 DNA Sequencer).

Pair-wise sequence alignments were performed to find the best-matching piecewise (local) or global alignments of two query sequences using the ClustalW program in the database and controls. The following primer sets were used during the PCR reaction (Table 3):

Table 3. Set of Primers for MTRR

rs1532268	
MTRR F	5'-GCAGAGGACAAGAGGAGATAAG-3'
MTRR R	5'-CGGGTAAGTGAGGACTCAAAG-3'

4.4. Statistical Analysis. The genotype and allele frequencies were determined using the GraphpadInstat 3 software. The obtained genotype data were analyzed and verified using the chi-square test. The comparison between observed and expected frequencies was made and tested on the population for Hardy–Weinberg equilibrium (a p -value of <0.05 is considered a statistically significant level).

4.5. Molecular Modeling and Dynamics Studies. Recently, we developed a complete 3D structure of the MTRR protein.²⁰ The structure was used to probe the effect of S202L population variation on the structure and dynamics of the protein. The S202L MTRR variant was built by mutating the 202nd serine residue to leucine using the mutagenesis toolkit of the Visual Molecular Dynamics (VMD) package. All the wild-type and S202L variant simulations were performed using the GROMACS 2018.1 package^{31,32} using the GROMOS 53a6 force field^{33,34} with the SPC/E water model.³⁵ The proteins were energy minimized in vacuo and then solvated in a cubic box of 105.5 Å dimension on each side with periodic boundary conditions. The box size was selected so that the minimum distance between any protein atom and

the box wall was at least 10 Å . Thirteen Na^+ ions were added to neutralize the charge of each system. Then, each system was energy minimized using the steepest-descent algorithm, followed by 1 ns position restraint dynamics in an NVT ensemble where the backbone atoms of the protein were only restrained. Finally, 500 ns production simulations were carried out for each system at 298 K in the NPT ensemble, where all the molecules were allowed to move freely. During the simulation, the temperature was kept constant by coupling to a thermostat using a V-rescale algorithm with a time constant for coupling set to 0.1 ps. The constant pressure of 1 bar was maintained using the isotropic Parrinello–Rahman barostat with the time constant for coupling set to 2 ps. Electrostatic interactions were calculated using the particle mesh Ewald summation (PME) method with default values for grid spacing. Three independent simulations of 500 ns for each system were carried out in an NPT ensemble using the same simulation parameters.

4.6. Bioinformatics Analysis. The sequence of the isoform A of human MTRR protein was retrieved from the UniProt database (UniProtKB-Q9UBK8, isoform A). Potential phosphorylation sites at serine, threonine, or tyrosine residues in the sequence and the specific kinases that act on a particular site were predicted by NetPhosK 1.0²⁸ and NetPhos 2.0.²⁹ Netphos uses an artificial neural network-based prediction method to predict phosphorylation sites in a sequence with a sensitivity of 69–96%. The algorithm was based on experimentally verified phosphorylation sites available from PhosphoBase. The data set contained 584 serine sites, 108 threonine sites, and 210 tyrosine sites from mammalian sources.

Possible sumoylation sites and SUMO-interaction motifs were predicted using the GPS-SUMO web server from the human MTRR sequence with a medium threshold for both sumoylation and SUMO interaction.³⁶ The program was developed based on the data set of 983 sumoylation sites in 545 proteins and 151 known SUMO interaction motifs from 80 proteins retrieved from the literature. A fourth-generation GPS algorithm integrated with the Particle Swarm Optimization (PSO) method was developed for training and prediction.

AUTHOR INFORMATION

Corresponding Authors

Biman Jana – School of Chemical Sciences, Indian Association for Cultivation of Science, Kolkata 700032, India; orcid.org/0000-0001-7684-1963; Email: pcbj@iacs.res.in

Madhusudan Das – Department of Zoology, University of Calcutta, Kolkata 700019, India; orcid.org/0000-0002-9051-3082; Email: madhuzoo@yahoo.com

Authors

Susanta Sadhukhan – Department of Zoology, University of Calcutta, Kolkata 700019, India

Subhajit Maity – Department of Zoology, University of Calcutta, Kolkata 700019, India; Department of Zoology, Ramakrishna Mission Vivekananda Centenary College, Kolkata 700118, India

Sandipan Chakraborty – Amity Institute of Biotechnology, Amity University Kolkata, Kolkata 700135, India; orcid.org/0000-0001-8759-1074

Silpita Paul – Department of Zoology, University of Calcutta, Kolkata 700019, India

Dinesh Munian – Department of Neonatology, Institute of Post Graduate Medical Education Research (IPGMER), Kolkata 700020, India

Arup Kumar Pattanayak – Department of Zoology, University of Calcutta, Kolkata 700019, India

Complete contact information is available at:

<https://pubs.acs.org/10.1021/acsomega.1c03563>

Notes

The authors declare no competing financial interest.

#S.S., S.M., and S.C. contributed equally.

ACKNOWLEDGMENTS

We are highly grateful to the West Bengal Science and Technology and Biotechnology (73 (sanc)-BT/P/Bdget/RD-05/2017 dt.27.03.2018) for financial support. B.J. wants to acknowledge financial support from the DST-SERB grant (ID: CRG/2020/000756).

REFERENCES

- (1) Greene, N. D. E.; Copp, A. J. Neural tube defects. *Annu. Rev. Neurosci.* **2014**, *37*, 221–242.
- (2) Rai, S.; Singh, R.; Pandey, S.; Singh, K.; Shinde, N.; Rai, S.; Prasad, R.; Shama, S. High incidence of neural tube defects in northern part of India. *Asian J. Neurosurg.* **2016**, *11*, 352–355.
- (3) Nikolopoulou, E.; Galea, G. L.; Rolo, A.; Greene, N. D. E.; Copp, A. J. Neural tube closure: cellular, molecular and biomechanical mechanisms. *Development* **2017**, *144*, 552–566.
- (4) De Marco, P.; Merello, E.; Mascelli, S.; Capra, V. Current perspectives on the genetic causes of neural tube defects. *Neurogenetics* **2006**, *7*, 201–221.
- (5) Yorulmaz, A.; Konak, M. Short-term results of patients with neural tube defects followed-up in the konya region, turkey. *Birth Defects Res.* **2019**, *111*, 261–269.
- (6) Hong, Z. H.; Jin, D. H.; Yuan, X. J.; Zhao, Y.; Lin, H. W.; Chen, J. Association of neural tube defects with congenital abnormalities of the urogenital system in a chinese cohort. *BMC Pediatr.* **2021**, *21*, 66.
- (7) Detrait, E. R.; George, T. M.; Etchevers, H. C.; Gilbert, J. R.; Vekemans, M.; Speer, M. C. Human neural tube defects: developmental biology, epidemiology, and genetics. *Neurotoxicol. Teratol.* **2005**, *27*, 515–524.
- (8) De Marco, P.; Merello, E.; Cama, A.; Kibar, Z.; Capra, V. Human neural tube defects: genetic causes and prevention. *BioFactors* **2011**, *37*, 261–268.
- (9) Whitehead, A. S.; Gallagher, P.; Mills, J. L.; Kirke, P. N.; Burke, H.; Molloy, A. M.; Weir, D. G.; Shields, D. C.; Scott, J. M. A Genetic defect in 5,10 methylenetetrahydrofolate reductase in neural tube defects. *QJM An Int. J. Med.* **1995**, *88*, 763–766.
- (10) Au, K. S.; Ashley-Koch, A.; Northrup, H. Epidemiologic and genetic aspects of spina bifida and other neural tube defects. *Dev. Disabil. Res. Rev.* **2010**, *16*, 6–15.
- (11) Mohamed, M. A.; Aly, H. Birth region, race and sex may affect the prevalence of congenital diaphragmatic hernia, abdominal wall and neural tube defects among us newborns. *J. Perinatol.* **2012**, *32*, 861–868.
- (12) Ebara, S. Nutritional role of folate. *Congenit. Anom. (Kyoto)*. **2017**, *57*, 138–141.
- (13) Steele, J. W.; Kim, S.-E.; Finnell, R. H. One-carbon metabolism and folate transporter genes: do they factor prominently in the genetic etiology of neural tube defects? *Biochimie* **2020**, *173*, 27–32.
- (14) Daly, L. E.; Kirke, P. N.; Molloy, A.; Weir, D. G.; Scott, J. M. Folate levels and neural tube defects: implications for prevention. *JAMA* **1995**, *274*, 1698–1702.
- (15) Crider, K. S.; Yang, T. P.; Berry, R. J.; Bailey, L. B. Folate and dna methylation: a review of molecular mechanisms and the evidence for folate's role. *Adv. Nutr.* **2012**, *3*, 21–38.
- (16) Milunsky, A.; Jick, H.; Jick, S. S.; Bruell, C. L.; MacLaughlin, D. S.; Rothman, K. J.; Willett, W. Multivitamin/folic acid supplementation in early pregnancy reduces the prevalence of neural tube defects. *JAMA* **1989**, *262*, 2847–2852.
- (17) Banerjee, R. V.; Matthews, R. G. Cobalamin-dependent methionine synthase. *FASEB J.* **1990**, *4*, 1450–1459.
- (18) Wolthers, K. R.; Lou, X.; Toogood, H. S.; Leys, D.; Scrutton, N. S. Mechanism of coenzyme binding to human methionine synthase reductase revealed through the crystal structure of the fnr-like module and isothermal titration calorimetry. *Biochemistry* **2007**, *46*, 11833–11844.
- (19) Martínez-Frías, M.-L.; Pérez, B.; Desviat, L. R.; Castro, M.; Leal, F.; Rodríguez, L.; Mansilla, E.; Martínez-Fernández, M.-L.; Bermejo, E.; Rodríguez-Pinilla, E.; Prieto, D.; Ugarte, M.; Group, E. W. Maternal polymorphisms 677c-t and 1298a-c of mthfr, and 66a-g mtrr genes: is there any relationship between polymorphisms of the folate pathway, maternal homocysteine levels, and the risk for having a child with down syndrome? *Am. J. Med. Genet. Part A* **2006**, *140A*, 987–997.
- (20) Sadhukhan, S.; Maity, S.; Chakraborty, S.; Paul, S.; Munian, D.; Kumar Pattanayak, A.; Jana, B.; Das, M. Structural insight into the effect of polymorphic variation on the functional dynamics of methionine synthase reductase: implications in neural tube defects. *Chem. Biol. Drug Des.* **2021**, *97*, 283–292.
- (21) Paul, S.; Sadhukhan, S.; Munian, D.; Bankura, B.; Das, M. Association of FOLH1, DHFR, and MTHFR gene polymorphisms with susceptibility of neural tube defects: a case control study from eastern india. *Birth Defects Res.* **2018**, *110*, 1129–1138.
- (22) Chakraborty, S.; Basu, S. Structural insight into the mechanism of amyloid precursor protein recognition by β -secretase 1: a molecular dynamics study. *Biophys. Chem.* **2015**, *202*, 1.
- (23) Chakraborty, S.; Chatterjee, B.; Basu, S. A mechanistic insight into the amyloidogenic structure of hiapp peptide revealed from sequence analysis and molecular dynamics simulation. *Biophys. Chem.* **2012**, 168–169.
- (24) Chakraborty, S.; Willett, H.; Biswas, P. K. Insight into estrogen receptor beta-beta and alpha-beta homo- and heterodimerization: a combined molecular dynamics and sequence analysis study. *Biophys. Chem.* **2012**, *170*, 42.
- (25) Hussein, H. A.; Borrel, A.; Geneix, C.; Petitjean, M.; Regad, L.; Camproux, A. C. Pockdrug-server: a new web server for predicting pocket druggability on holo and apo proteins. *Nucleic Acids Res.* **2015**, *43*, W436–W442.
- (26) Hubbard, P. A.; Shen, A. L.; Paschke, R.; Kasper, C. B.; Kim, J.-J. P. NADPH-cytochrome P450 oxidoreductase: structural basis for hydride and electron transfer. *J. Biol. Chem.* **2001**, *276*, 29163–29170.
- (27) Piovesan, D.; Minervini, G.; Tosatto, S. C. E. The RING 2.0 web server for high quality residue interaction networks. *Nucleic Acids Res.* **2016**, *44*, W367–W374.
- (28) Blom, N.; Sicheritz-Pontén, T.; Gupta, R.; Gammeltoft, S.; Brunak, S. Prediction of post-translational glycosylation and phosphorylation of proteins from the amino acid sequence. *Proteomics* **2004**, *4*, 1633–1649.
- (29) Blom, N.; Gammeltoft, S.; Brunak, S. Sequence and structure-based prediction of eukaryotic protein phosphorylation sites. *E. cohen. J. Mol. Biol.* **1999**, *294*, 1351–1362.
- (30) Pishva, S. R.; Vasudevan, R.; Etemad, A.; Heidari, F.; Komara, M.; Ismail, P.; Othman, F.; Karimi, A.; Sabri, M. R. Analysis of MTHFR and MTRR gene polymorphisms in iranian ventricular septal defect subjects. *Int. J. Mol. Sci.* **2013**, *14*, 2739–2752.
- (31) Van Der Spoel, D.; Lindahl, E.; Hess, B.; Groenhof, G.; Mark, A. E.; Berendsen, H. J. C. GROMACS: fast, flexible, and free. *J. Comput. Chem.* **2005**, *26*, 1701–1718.
- (32) Kutzner, C.; Páll, S.; Fechner, M.; Esztermann, A.; Groot, B. L.; Grubmüller, H. More bang for your buck: improved use of gpu nodes for GROMACS 2018. *J. Comput. Chem.* **2019**, *40*, 2418–2431.
- (33) Cao, Z.; Lin, Z.; Wang, J.; Liu, H. Refining the description of peptide backbone conformations improves protein simulations using the GROMOS 53A6 force field. *J. Comput. Chem.* **2009**, *30*, 645–660.

- (34) Oostenbrink, C.; Soares, T. A.; van der Vegt, N. F. A.; van Gunsteren, W. F. Validation of the S3A6 GROMOS force field. *Eur. Biophys. J.* **2005**, *34*, 273–284.
- (35) Berendsen, H. J. C.; Grigera, J. R.; Straatsma, T. P. The missing term in effective pair potentials. *J. Phys. Chem.* **1987**, *91*, 6269–6271.
- (36) Zhao, Q.; Xie, Y.; Zheng, Y.; Jiang, S.; Liu, W.; Mu, W.; Liu, Z.; Zhao, Y.; Xue, Y.; Ren, J. GPS-SUMO: A tool for the prediction of sumoylation sites and sumo-interaction motifs. *Nucleic Acids Res.* **2014**, *42*, W325–W330.